PERGAMON

Vision Research 42 (2002) 1611–1617

Vision Research

www.elsevier.com/locate/visres

Ocular wave-front aberration statistics in a normal young population

José Francisco Castejón-Mochón, Norberto López-Gil *, Antonio Benito, Pablo Artal

Laboratorio de Óptica, Departamento de Física, Universidad de Murcia, Campus de Espinardo, Edificio C, 30071 Murcia, Spain

Received 15 June 2001; received in revised form 2 January 2002

Abstract

Monochromatic ocular aberrations in 108 eyes of a normal young population ($n = 59$) were studied. The wave-front aberration were obtained under natural conditions using a near-infrared Shack–Hartmann wave-front sensor. For this population and a 5 mm pupil, more than 99% of the root-mean square wave-front error is contained in the first four orders of a Zernike expansion and about 91% corresponds only to the second order. Comparison of wave-fronts aberrations from right and left eye in 35 subjects, showed a good correlation between most of the second- and third-order terms and a slight (but not clear) tendency for mirror symmetry between eyes.

Keywords: Wave-front aberration; Retinal image quality; Human eye

1. Introduction

The ocular wave-front aberration (OWA) is normally represented as the departure, from a perfect plane wave, of the wave-front generated by the light that leaves the eye coming from a point source focused on the fovea. The OWA provides useful information about the eye's imaging abilities in monochromatic light. From the estimates of the OWA (Charman, 1991), one can compute both the eye's point spread function and the modulation transfer function (Goodman, 1996).

The OWA was first measured by Smirnov (1961) using a vernier alignment technique. The cross-cylinder aberroscope is another older technique for measuring the OWA (Howland & Howland, 1976). More recently, a number of other methods for measuring ocular aberrations have been proposed. Among these are: the objective aberroscope (López-Gil & Howland, 1999; Walsh, Charman, & Howland, 1984); the spatially resolved refractometer (Webb, Penney, & Thompson, 1992); computations from retinal images (Artal, Iglesias, López-Gil, & Green, 1995; Iglesias, Berrio, & Artal, 1998); and the Shack–Hartmann (S–H) sensors (Liang, Grimm, Goelz, & Bille, 1994; Liang & Williams, 1997; Prieto, Vargas-Martín, Goelz, & Artal, 2000). Recent improvements of the S–H sensor allow it to measure the OWA several times a second (Hofer, Artal, Singer, Aragon, & Williams, 2001a). This has allowed a closed-loop correction of the OWA in the living eye (Fernández, Iglesias, & Artal, 2001; Hofer et al., 2001b). These new S–H techniques, until recently laboratory prototypes, are currently being incorporated into clinical instruments (Mrochen, Kaemmerer, & Seiler, 2001) and therefore the number of eyes on which the OWA has been measured has increased dramatically in the last years. The new instruments allow one to obtain data of the OWA in a large population (hundreds of eyes) in relatively short period of time (Bradley, Hong, Thibos, Cheng, & Miller, 2001; Porter, Guirao, Cox, & Williams, 2001). The interest of these studies is to establish the range of aberrations in different normal populations.

Other laboratories have also recently published results of OWA measurements in relatively large population of normal subjects. Porter et al. (2001), studied a population covering a wide range of ages, and Bradley et al. (2001), measured a young population under cyclopegia. In the present communication, we present OWA measurements obtained in a population of university students (20–30 years old) under natural viewing conditions without optical correction.

* Corresponding author. Fax: +34-96-836-3528.
E-mail address: norberto@um.es (N. López-Gil).

0042-6989/02/$ - see front matter
PII: S0042-6989(02)00085-8

2. Methods

The measurements of the OWA's in the population were performed with a near-infrared S–H sensor. A schematic diagram of the set-up used is in Fig. 1.

A super-luminiscent diode (SLD), partially collimated and emitting at 784 nm with a spectral bandwidth of 44 nm, produced a beacon source on the retina. The light reflected from the retina was used to measure the OWA. The eye's pupil was conjugate with mirror M_2 by means of L_1 and L_2 and with the microlenses array by means of lenses L_3 and L_4. Between L_1 and L_2 an optical subsystem consisting of two pairs of mirrors (M_3–M_6) were placed. This subsystem was only used to test the defocus measurements performances of the system (see below). A CCD camera, Dalsa CA-D4, with a pixel size of 12 μm was placed in the focal plane of the microlens array to record the S–H images. A He–Ne laser (L) emitting in the visible range (633 nm) was used together with a removable mirror (RM) for alignment.

Although the low coherence of the SLD helped to partially avoid speckle in the S–H images, this is still present with the exposure time (500 ms) typically used. The residual speckle could be removed by using a spinning mirror M_2 (Aragón, López-Gil, & Artal, 1999) that scans and de-scans the beam before and after the light reaches the retina (similar to the strategy suggested by Hofer et al. (2001a)). In order to have a large dynamic range in measuring aberrations, we used an array of microlenses with short focal length ($f' = 6.3$ mm). This has three advantages. First, it avoided the use of the scanning mirror (M_2 does not need to spin) because speckle plays a small role in detecting the centroid. Second, it allowed accurate measurements with defocus up to ±9 D. Third, it increases the signal to noise ratio of the S–H images. As an example, Fig. 2 shows two S–H images obtained with the same exposure time (500ms) in the same subject but with two different microlens focal lengths (40 and 6.3 mm). Note the increase in contrast obtained by decreasing the focal length.

The corneal reflex of the SLD can be seen in one of the S–H images (Fig. 2b) and is concentrated on a small area of the S–H image. This reflex affected only to a few number of spots that are not included in the computations of the OWA. Because of the short focal length used, small errors in positioning of the microlenses have large affects on the aberration (Pfund, Lindlein, & Schwider, 1998). The impact of the microlenses misalignment is eliminated by using a reference image during processing. The reference image was recorded by placing a diffuser between mirrors M_5 and M_6, a position conjugate with the microlenses focal plane (CCD

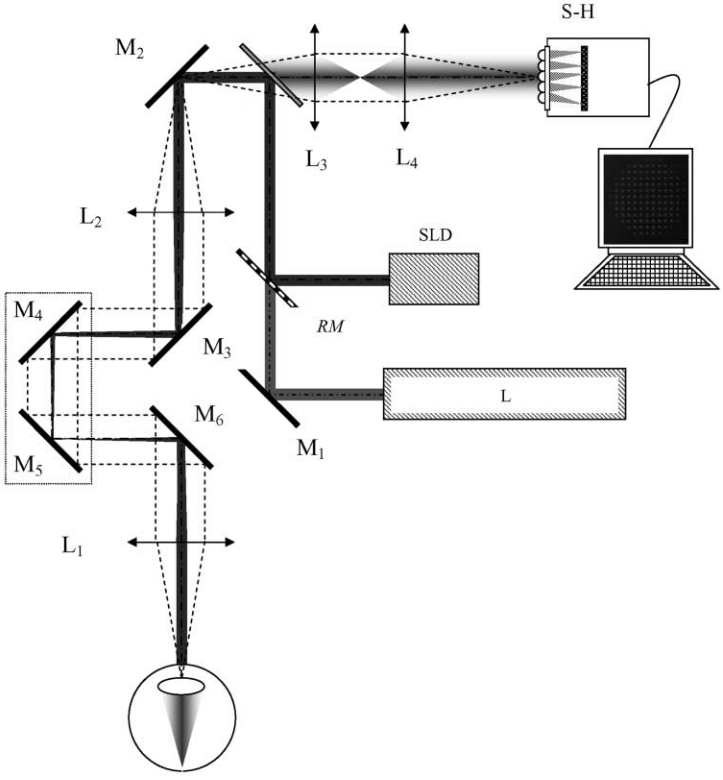

Fig. 1. Experimental set-up. L, He–Ne laser (632.8 nm); M_1–M_6, mirrors; RM, removable mirror; BS, beam splitter; SLD, super-luminiscent infrared laser diode (784 nm); L_1–L_4 achromatic lenses; S–H, Shack–Hartmann sensor (microlens array + CCD camera).

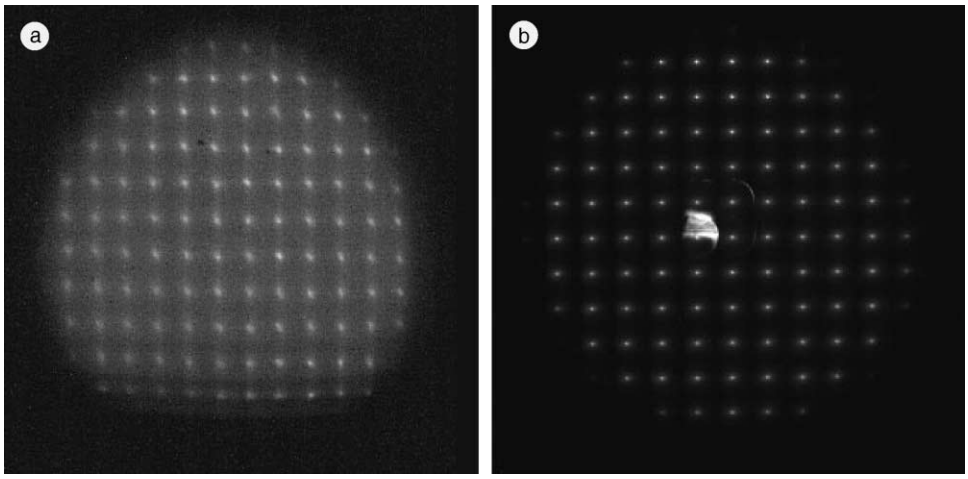

Fig. 2. S–H images obtained from the same eye with microlenses with focal length of (a) 40 mm and (b) 6.3 mm.

plane). In addition, a robust sub-pixel centroiding algorithm was used (see Prieto et al., 2000 for further details).

To calibrate the sensor we measured a series of precisely known induced amounts of defocus and spherical aberration. Defocus was introduced by displacing the optical subsystem mentioned before. In particular, for a pupil diameter of 5 mm, the increase of 1 mm of the optical path between lenses L_1 and L_2 (both with a 20 cm focal length) theoretically changes the value of the defocus Zernike coefficient (Z_2^0) by 0.045 μm, corresponding to 0.050 D of defocus. Fig. 3 shows the calibration results for defocus. The line fitted in Fig. 3 had a slope of 0.047 μm/mm ($R = 0.999$), close to the expected value (0.045 μm/mm). That is, for every diopter of defocus generated by the optical subsystem, we measured 1.05 D. We introduced phase plates with known spherical aberration (López-Gil, Howland, Howland, Charman, & Applegate, 1998), in particular, 0.028 and −0.028 μm for a 5 mm pupil diameter. We measured values of 0.021 and −0.022 μm, for each lens respectively.

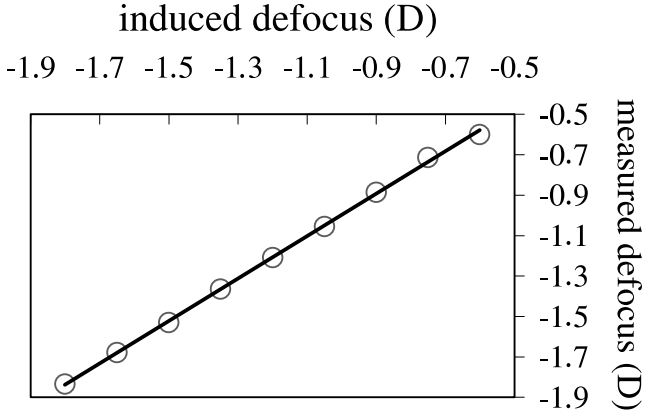

Fig. 3. Defocus calibration.

We measured the OWA in both eyes of most of the 59 subjects (108 eyes). The subjects age ranged from 20 to 30 years old, with a mean value of 24 ± 3 (SD) years. All subjects were students at Murcia University with normal vision and without any known ocular pathology. All the volunteer subjects signed an informed consent after the nature and all possible consequences of the study had been explained.

The irradiance on the cornea was lower than 27 μW/cm^2 during a typical exposure duration of 5 s (10 frames at 500 ms/frame). This is approximately two orders of magnitude less than the maximum permissible exposure time for continuous viewing for this wavelength, according to the American National Standards (ANSI Z136.1, 1993). For each eye, 10 S–H images were recorded under natural viewing conditions with a fixation target at the infinity. The wave-front aberrations were calculated from the last frame in the series, except when there was a blink at the very last moment. The OWA were represented with a Zernike polynomials expansion (Noll, 1976) up to fourth, fifth, sixth, seventh and eighth order for 3, 4, 5, 6 and 7 mm pupil diameters, respectively. Although a very dim room ambient light was used, in a few subjects we could not process the images for pupil diameter larger than 5 mm because the subjects natural small pupil diameter.

3. Results

Fig. 4 shows the mean value of every Zernike term for all the subjects measured using a pupil of 5 mm in diameter.

The results show a large (relative to the mean) dispersion in all Zernike coefficients. Myopic defocus (Z_2^0) and astigmatism "with the rule" (Z_2^2) were the dominant aberrations, which also exhibited the greatest inter-subject variability. For every Zernike term beyond second

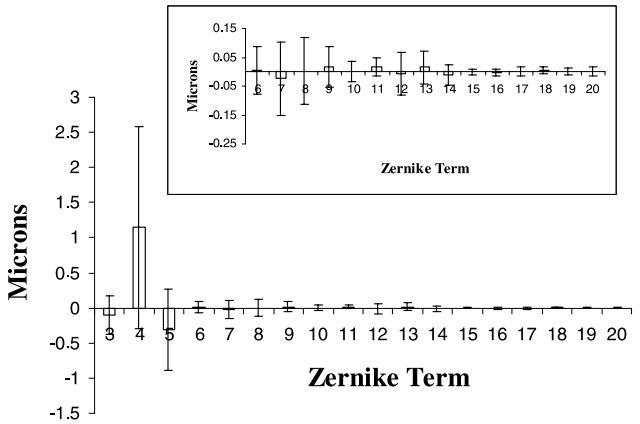

Fig. 4. Mean and standard deviation for each term of the Zernike expansion up to the fifth order. Number in the *X*-axis represents the *j*-index related to each Zernike term. The inserted small figure shows the values of higher-order terms with a different scale.

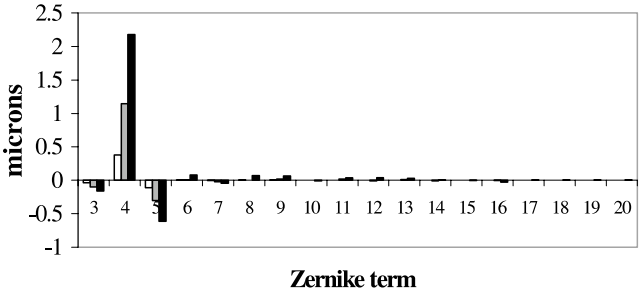

Fig. 5. Mean value of each term of the Zernike expansion up to the fifth order for a pupil diameter of 3 mm (open bars), 5 mm (gray bars) and 7 mm (black bars). Numbers in the *X*-axis represent the *j*-index related to each Zernike term.

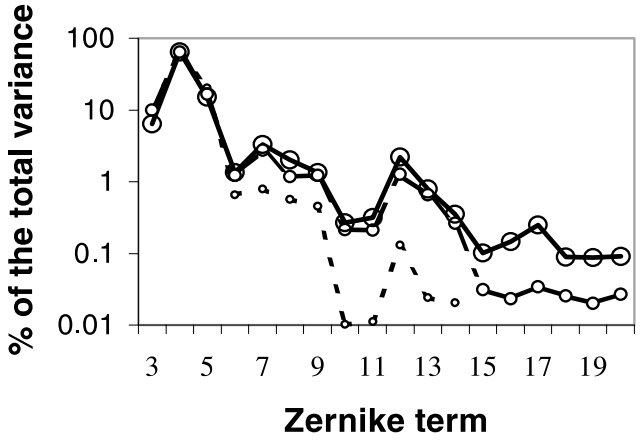

Fig. 6. Percentage of the total variance (excluding piston and prisms) of each Zernike term for a pupil diameter of 3 mm (···), 5 mm (- - -) and 7 mm (—). Number in the *X*-axis represents the *j*-index related to each Zernike term.

Table 1
Impact of each Zernike order on the total RMS for three different pupil sizes

	3 mm	5 mm	7 mm
Total RMS	0.5255 μm	1.4901 μm	2.9240 μm
Second order	97.3%	90.8%	86.2%
Third order	2.5%	6.4%	8.0%
Fourth order	0.2%	2.6%	3.9%
Fifth order		0.2%	1.5%

Percentages were obtained by averaging the percentage of each subject for each coefficient and regrouping by orders. No fifth-order fitting was done for a 3 mm pupil diameter due to the lacked of data.

order, the mean value for all the subjects measured was lower than 0.03 μm. For pupils of 3, 4, 5, 6 and 7 mm, the calculated mean total root mean squared (excluding piston and tilts) of the wave-front (total RMS), were 0.53, 0.94, 1.49, 2.2 and 2.9 μm, respectively. Fig. 5 shows the mean value of each Zernike coefficient for three different pupil diameters (3, 5 and 7 mm).

In order to know the weight of each Zernike term in the variance of the OWA, we computed a percentage factor, c_j, as:

$$\frac{c_j^2}{\sum_{i=3}^{20} c_j^2} \times 100$$

where single indexing scheme, c_j, of the OSA-standard Zernike coefficient notation is used for clarity (Thibos, Applegate, Schwiegerling, & Webb, 2000). The value in the denominator represents the variance of the OWA obtained from the third (piston and tilt coefficients were not included) to 20th Zernike coefficient, corresponding to the end of the fifth-order Zernike expansion. The values of those percentages are represented in Fig. 6, computed from pupil diameters of 3, 5 and 7 mm.

Table 1 represents the average total RMS for three different pupil sizes (diameters of 3, 5 and 7 mm), as well as the percentages calculated for each Zernike order. Thus, low-order aberration is represented by second-order Zernike coefficients with a suffix index from 3 to 5 (corresponding to defocus and astigmatism). High-order aberrations correspond to coefficients with higher indexes. In particular, index form 6 to 9 for third order, from 10 to 14 for fourth order and 15 to 20 for the fifth order (Thibos et al., 2000).

We also studied the relation among Zernike coefficients in both eyes of each subject. A total of 49 pairs of eyes were measured. However, due to the fact that measurements were obtained under natural conditions without any kind of cycloplegia, data for a 7 mm pupil where only taken in 35 pairs. We present the data of those 35 pairs of eyes in Fig. 7. Values of right and left eyes have been represented in the *X* and *Y*-axes, respectively. A linear regression coefficient (R) was computed for each Zernike term for all the subject analyzed. Values are shown in Table 2.

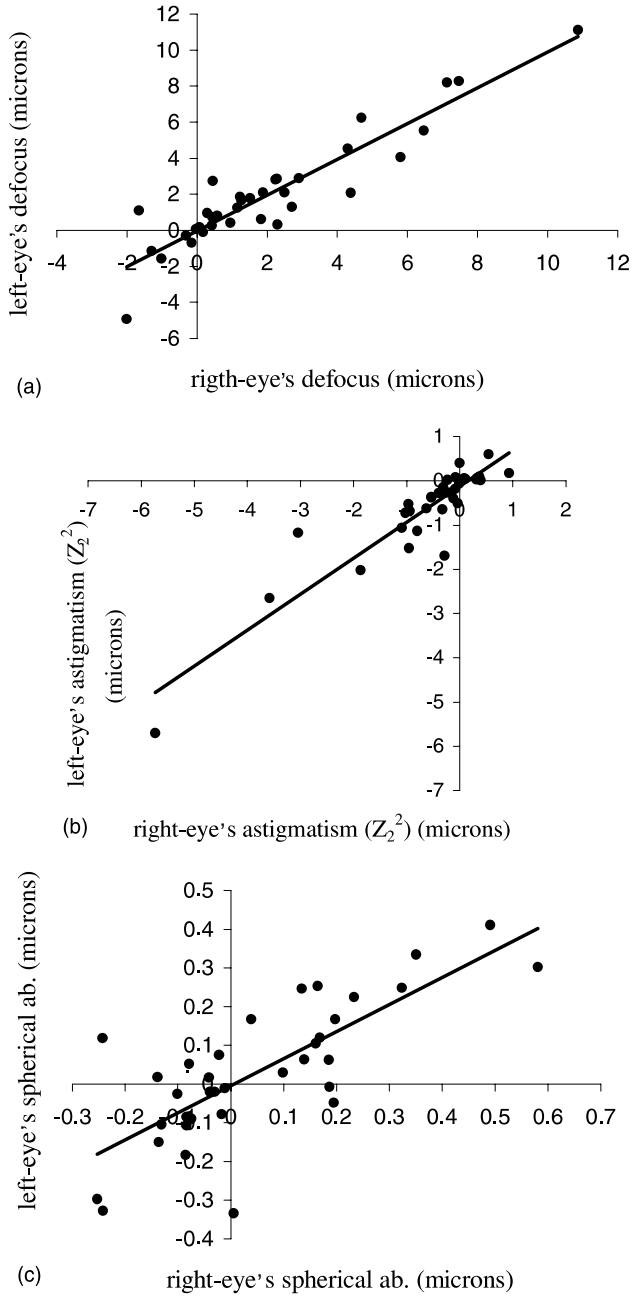

Fig. 7. Correlation between right (X-axis) and left (Y-axis) eye of a 7 mm pupil diameter, for defocus (a), astigmatism (Z_2^2) (b), and third order spherical aberration (c). Each point represents a subject.

In general, second-order terms and third-order spherical aberration were found to be well correlated in both eyes. In the case of the astigmatism (Z_2^{-2}), we found a small correlation ($R = -0.2$) between both eyes, while the correlations for astigmatism with and without the rule is much higher ($R > 0.9$).

Besides third-order spherical aberration, for high-order aberrations, the higher correlation was found for coma, being in general small for the rest of Zernike terms. Correlation between eyes were significant ($p < 0.05$) for most of the second- and third-order coefficients (see Table 2).

4. Conclusions and discussion

We measured the OWA in a young population of University students by using a near-infrared aberrometer (S–H type). The mean values and standard deviation (SD) of the RMS for a pupil size of 5 mm were 1.49 and 1.32 μm, respectively. For a 5 mm pupil, the 99.8% of the total RMS was contained in a expansion up to the fourth order. This indicates that most of the wave-front aberration is well represented using only the first 15th Zernike polynomial terms in the case of small or medium pupil sizes.

Second-order, myopic defocus ($Z_2^0 > 0$) and astigmatism with the rule ($Z_2^2 < 0$) were found to be the dominant aberrations, with a huge inter-subject variability. The mean value for those two coefficients for a five-pupil radius was 1.14 and −0.27 μm with SD 1.44 and 0.30 μm, respectively.

Bradley et al. (2001) and Porter et al. (2001) have also observed a high inter-subject variability. Moreover, the percentages of RMS for different orders reported for their two groups were similar to what was found in this study. In particular, Porter and collaborators found that, for a 5.7 mm pupil, 92.7% and 98.6% of the total RMS is in the first two and three orders, respectively (Porter et al., 2001). In the present study, we obtained values of 90.8% and 97.2% in the first two and three orders respectively for a 5 mm pupil, and 86.2% and 94.2% for a 7 mm pupil. The small differences could due to the fact that there is a 17 years in the mean ages of the two populations with the fact that higher-order aberrations increase with age (Guirao et al., 1999). The differences are smaller when comparing our results with the young corrected group (26.1 years in average) studied by Bradley et al. (2001). In that study, the authors found that, for a 6 mm pupil, the 99% of the total RMS is contained in the first fourth orders. This value is very similar to this study: 99.8% and 98.1% for 5 and 7 mm pupil, respectively (see Table 1).

As is well known the impact of high-order aberrations increased with pupil size. More precisely, we found an increase from 2.7% to 13.8% for pupil size of 3–7 mm. The change in the values of the total RMS with pupil size grew with approximately the second power of the pupil radius. That is, there is a direct relation between total RMS and the pupil area. Fig. 8 presents the total RMS obtained for different pupil radius. The data has been fitted by a quadratic curve and had a regression coefficient $R^2 = 0.999$. This result is not surprising taking into account that most of the aberration is due to the second order (with a square radius dependency). However, the fit to a quadratic might not be so good in other

Table 2
Relation of Zernike coefficients between right and left eye for a 7 mm pupil diameter

Order	Zernike term	Polynomial	R	Slope	p-Value
Second order	Z_2^{-2} (C_3)	$\rho^2 \sin 2\phi$	−0.2	−0.18	0.25
	Z_2^0 (C_4)	$2\rho^2 - 1$	0.92	0.99	0.00
	Z_2^2 (C_5)	$\rho^2 \cos 2\phi$	0.91	0.81	0.00
Third order	Z_3^{-3} (C_6)	$\rho^3 \sin 3\phi$	0.63	0.49	0.00
	Z_3^{-1} (C_7)	$(3\rho^3 - 2\rho) \sin \phi$	0.65	0.49	0.00
	Z_3^1 (C_8)	$(3\rho^3 - 2\rho) \cos \phi$	0.6	0.63	0.00
	Z_3^3 (C_9)	$\rho^3 \cos 3\phi$	−0.16	−0.20	0.34
Fourth order	Z_4^{-4} (C_{10})	$\rho^4 \sin 4\phi$	0.15	0.22	0.38
	Z_4^{-2} (C_{11})	$(4\rho^4 - 3\rho^2) \sin 2\phi$	−0.09	−0.09	0.60
	Z_4^0 (C_{12})	$(6\rho^4 - 6\rho^2 + 1)$	0.77	0.70	0.00
	Z_4^2 (C_{13})	$(4\rho^4 - 3\rho^2) \cos 2\phi$	0.40	0.40	0.02
	Z_4^4 (C_{14})	$\rho^4 \cos 4\phi$	0.56	0.98	0.00
Fifth order	Z_5^{-5} (C_{15})	$\rho^5 \sin 5\phi$	0.44	0.58	0.01
	Z_5^{-3} (C_{16})	$(5\rho^5 - 4\rho^3) \sin 3\phi$	−0.11	−0.10	0.53
	Z_5^{-1} (C_{17})	$(10\rho^5 - 12\rho^3 + 2\rho) \sin \phi$	−0.03	−0.02	0.87
	Z_5^1 (C_{18})	$(10\rho^5 - 12\rho^3 + 2\rho) \cos \phi$	−0.19	−0.23	0.27
	Z_5^3 (C_{19})	$(5\rho^5 - 4\rho^3) \cos 3\phi$	0.21	0.43	0.23
	Z_5^5 (C_{20})	$\rho^5 \cos 5\phi$	−0.06	−0.05	0.75

Regression coefficients and slope values are obtained after fitting to a straight line (see in the text). Third column does not include normalization coefficient.

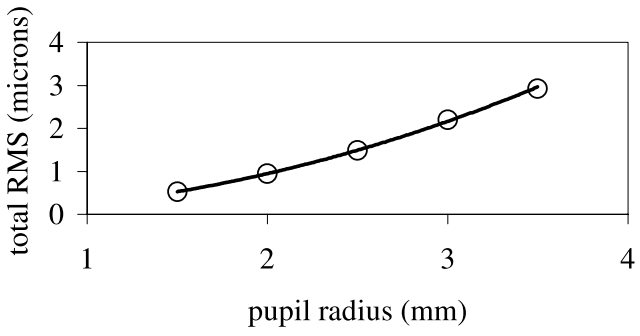

Fig. 8. Relation between pupil radius and the total RMS. Data points has been fitted by a quadratic function.

populations, for instance older subjects (Guirao et al., 1999) or pathological eyes (López-Gil, Marín, Castejón-Mochón, Benito, & Artal, 2001) were higher-order aberrations are larger.

For a 7 mm pupil, second and third order are better correlated between right and left eyes, except for oblique astigmatism (Z_2^{-2}) ($R = -0.2$, $p = 0.25$) and the triangular astigmatism represented by the ninth Zernike polynomial ($R = -0.16$, $p = 0.34$). Other Zernike terms are not so well correlated except for third-order spherical aberration ($R = 0.77$, $p = 0.00$) and the 14th Zernike polynomial ($R = 0.56$, $p = 0.00$). Half of Zernike terms are significantly correlated for $p = 0.02$ (9 out of 18 Zernike terms), while for $p = 0.01$, eight out of 18 terms are significantly correlated.

A rotation of the angular coordinates (ϕ) of 180° on the OWA will change the sign of the coefficients corresponding to the Zernike polynomial which depend on the $\cos((n+1)\phi)$ and $\sin(n\phi)$, with n even. In Table 2, those coefficient are: Z_2^{-2}, Z_3^1, Z_3^3, Z_4^{-4}, Z_4^{-2}, Z_5^1, Z_5^3 and Z_5^5. Thus, a mirror (chiral) symmetry of the OWA between eyes, as suggested by Liang and Williams (1997) and studied by Porter et al. (2001), would produce a negative slope value for those coefficients in Table 2. The results presented in Table 2, show five out of eighth of those coefficients with a negative value. However, some of them had high p values and low regression coefficient (R), specially for coefficients corresponding to fifth order in which aberrations are very small.

The apparently lack of symmetry for the oblique astigmatism term (Z_2^{-2}) can be explained by comparing the astigmatism amplitude and axis between right and left eyes computed from both astigmatism Zernike terms (Z_2^2 and Z_2^{-2}). That comparison shows that symmetry on axis direction increased with astigmatism module. In addition, we did not find a negative slope value for the third-order Zernike coefficient corresponding to coma (Z_3^1) where the correlation between eyes was significant ($p = 0.00$). Thus, the population study do not show a clear mirror symmetry of the OWA between right and left eyes, as has been recently reported before by Porter et al. (2001), but rather a slight tendency in this direction.

In summary, this paper describes the statistical results of wave aberration measurements made on the eyes of a young student population for several different pupil sizes. This kind of study will have an impact in clinical ophthalmology. With the increasing number of patients of all ages who are receiving refractive surgical procedures, it is important to establish aberration standards

that are indicative of normal individuals. This will be a useful tool to evaluate the optical and visual outcomes in refractive surgery.

Acknowledgements

The authors thank to all the students that have participated in the study founded by grants DGES-Spain (PB97-1056) and EU-BRITE_EURAM Project (BE97-4608). Thanks to Daniel Green for his support on reviewing the manuscript as well as the two anonymous reviewers for their critical comments.

References

ANSI Z136.1. (1993). American National Standard for the Safe Use of Lasers.

Aragón, J. L., López-Gil, N., & Artal, P. (1999). Real-time double-pass system to study the dynamics of the eye's optical performance. PhO'99. *EOS Topical Meeting Digest Series, 23*, 49–50.

Artal, P., Iglesias, I., López-Gil, N., & Green, D. G. (1995). Double-pass measurements of the retinal-image quality with unequal entrance and exit pupil sizes and the reversibility of the eye's optical system. *Journal of the Optical Society of America A, 12*, 2358–2366.

Bradley, A., Hong, X., Thibos, L. N., Cheng, X., & Miller, D. T. (2001). The statistics of monochromatic aberrations from 200 healthy young eyes [ARVO abstract]. *Investigative Ophthalmology and Visual Science, 42*(4), B175, Abstract no. 862.

Charman, W. N. (1991). Wavefront aberration of the eye: a review. *Optometry and Vision Science, 68*, 574–583.

Fernández, E. J., Iglesias, I., & Artal, P. (2001). Closed-loop adaptive optics in the human eye. *Optics Letters, 26*, 746–749.

Goodman, J. W. (1996). *Introduction to Fourier optics* (2nd ed.). New York: McGraw-Hill.

Guirao, A., Gonzalez, C., Redondo, M., Geraghty, E., Norrby, S., & Artal, P. (1999). Average optical performance of the human eye as a function of age in a normal population. *Investigative Ophthalmology and Visual Science, 40*, 197–202.

Hofer, H., Artal, P., Singer, B., Aragon, J. L., & Williams, D. R. (2001a). Dynamics of the eye's wave aberration. *Journal of the Optical Society of America A, 18*, 497–506.

Hofer, H., Chen, L., Yoon, G. Y., Singer, B., Yamauchi, Y., & Williams, D. R. (2001b). Performance of the Rochester 2nd generation adaptive optics system for the eye. *Optics Express, 8*, 631–643, http://www.opticsexpress.org/oearchive/source/31887. htm.

Howland, B., & Howland, H. C. (1976). Subjective measurement of high-order aberrations of the eye. *Science, 193*, 580–582.

Iglesias, I., Berrio, E., & Artal, P. (1998). Estimates of the ocular wave aberration from pairs of double-pass retinal images. *Journal of the Optical Society of America A, 15*, 2466–2476.

Liang, J., Grimm, B., Goelz, S., & Bille, J. F. (1994). Objective measurement of wave aberrations of the human eye with the use of a Hartmann–Shack wave-front sensor. *Journal of the Optical Society of America A, 11*, 1949–1957.

Liang, J., & Williams, D. R. (1997). Aberrations and retinal image quality of the normal human eye. *Journal of the Optical Society of America A, 14*, 2873–2883.

López-Gil, N., & Howland, H. C. (1999). Measurement of the eye's near infrared wave-front aberration using the objective crossed-cylinder aberroscope technique. *Vision Research, 39*, 2031–2037.

López-Gil, N., Howland, H. C., Howland, B., Charman, N., & Applegate, R. (1998). Generation of third-order spherical and coma aberration using radially symmetric fourth-order lenses. *Journal of the Optical Society of America A, 15*, 2563–2571.

López-Gil, N., Marín, J. M., Castejón-Mochón, J. F., Benito, A., & Artal, P. (2001). Ocular and corneal aberrations after corneal transplantation. *Investigative Ophthalmology and Visual Science, 42*(4), S529.

Mrochen, M., Kaemmerer, M., & Seiler, T. (2001). Clinical results of wavefront-guided laser in situ keratomileusis 3 months after surgery. *Journal of Cataract Refractive Surgery, 27*, 201–207.

Noll, R. J. (1976). Zernike polynomials and atmospheric turbulence. *Journal of the Optical Society of America, 66*, 207–211.

Pfund, J., Lindlein, N., & Schwider, J. (1998). Misalignment effects of the Hartmann–Shack sensor. *Applied Optics, 37*(1).

Porter, J., Guirao, A., Cox, I. G., & Williams, D. R. (2001). Monochromatic aberrations of the human eye in a large population. *Journal of the Optical Society of America A, 18*, 1793–1803.

Prieto, P. M., Vargas-Martín, F., Goelz, S., & Artal, P. (2000). Analysis of the performance of the Hartmann–Shack sensor in the human eye. *Journal of the Optical Society of America A, 17*, 1388–1398.

Smirnov, M. S. (1961). Measurement of the wave aberration of the human eye. *Biofizika, 6*, 776–795.

Thibos, L. N., Applegate, R. A., Schwiegerling, J. T., & Webb, R. (2000). VSIA Standards Taskforce Members. In V. Lakshminarayana (Ed.), *Standards for Reporting the Optical Aberrations of the Eyes. OSA Trends in Optics and Photonics. Vol. 35: Vision Science and Its Applications* (pp. 232–244). Washington, DC: Optical Society of America.

Walsh, G., Charman, W. N., & Howland, H. C. (1984). Objective technique for the determination of monochromatic aberrations of the human eye. *Journal of the Optical Society of America A, 1*, 987–992.

Webb, R. H., Penney, C. M., & Thompson, K. P. (1992). Measurement of ocular local wave-front distortion with a spatially resolved refractometer. *Applied Optics, 311*, 3678–3686.